PROCEEDINGS OF SPIE

SPIEDigitalLibrary.org/conference-proceedings-of-spie

Hyperspectral imaging with near-infrared-enabled mobile phones for tissue oximetry

Jonathan L. Lin, Pejhman Ghassemi, Yu Chen, Joshua Pfefer

Jonathan L. Lin, Pejhman Ghassemi, Yu Chen, Joshua Pfefer, "Hyperspectral imaging with near-infrared-enabled mobile phones for tissue oximetry," Proc. SPIE 10485, Optics and Biophotonics in Low-Resource Settings IV, 104850C (13 February 2018); doi: 10.1117/12.2290870

SPIE.

Event: SPIE BiOS, 2018, San Francisco, California, United States

Hyperspectral Imaging with Near-Infrared-Enabled Mobile Phones for Tissue Oximetry

Jonathan L. Lin[1], Pejhman Ghassemi[1], Yu Chen[2], and Joshua Pfefer[1]
[1]Center for Devices and Radiological Health, U.S. Food and Drug Administration
10903 New Hampshire Avenue, Silver Spring, MD USA 20993
[2]Fischell Department of Bioengineering, University of Maryland, College Park
University of Maryland, College Park, MD USA 20742

ABSTRACT

Hyperspectral reflectance imaging (HRI) is an emerging clinical tool for characterizing spatial and temporal variations in blood perfusion and oxygenation for applications such as burn assessment, wound healing, retinal exams and intra-operative tissue viability assessment. Since clinical HRI-based oximeters often use near-infrared (NIR) light, NIR-enabled mobile phones may provide a useful platform for future point-of-care devices. Furthermore, quantitative NIR imaging on mobile phones may dramatically increase the availability and accessibility of medical diagnostics for low-resource settings. We have evaluated the potential for phone-based NIR oximetry imaging and elucidated factors affecting performance using devices from two different manufacturers, as well as a scientific CCD. A broadband light source and liquid crystal tunable filter were used for imaging at 10 nm bands from 650 to 1000 nm. Spectral sensitivity measurements indicated that mobile phones with standard NIR blocking filters had minimal response beyond 700 nm, whereas one modified phone showed sensitivity to 800 nm and another to 1000 nm. Red pixel channels showed the greatest sensitivity up to 800 nm, whereas all channels provided essentially equivalent sensitivity at longer wavelengths. Referencing of blood oxygenation levels was performed with a CO-oximeter. HRI measurements were performed using cuvettes filled with hemoglobin solutions of different oxygen saturation levels. Good agreement between absorbance spectra measured with mobile phone and a CCD cameras were seen for wavelengths below 900 nm. Saturation estimates showed root-mean-squared-errors of 5.2% and 4.5% for the CCD and phone, respectively. Overall, this work provides strong evidence of the potential for mobile phones to provide quantitative spectral imaging in the NIR for applications such as oximetry, and generates practical insights into factors that impact performance as well as test methods for performance assessment.

Keywords: hyperspectral reflectance imaging, near-infrared, oximetry, mobile phone

1. INTRODUCTION

Mobile phones are a widely available, highly adaptable, and portable platform for communication, computation, and imaging, leading to their great popularity. They are constantly improving, with advances to their computational power and camera quality every year. There is growing interest in their applicability as an imaging platform, with studies discovering their potential for visible wavelength fluorescence microscopy[1], fundus imaging[2,3], photoplethysmography[4], and skin cancer detection[5]. Their appeal has also resulted in several mobile phone-based commercial medical devices, including an otoscope[6] and an ophthalmoscope[7]. While mobile phone cameras are based on CMOS detectors, which can view light across the visible and NIR spectrum, manufacturers add filters that block light in the NIR range to improve their performance for consumer photography. Recently, we started to explore the possibilities offered by implementing phone cameras without NIR blocking filters in a proof of principle study for mobile NIR fluorescence imaging with a clinical contrast agent in phantom and animal models[8]. Widening their spectral range provides mobile phones with much greater sensing capabilities for a variety of biomedical applications, such as cancer identification[9] and endoscopy[10,11].

Another particularly exciting application is hyperspectral reflectance imaging (HRI), which enables identification of chromophore contributions through their unique spectral signatures. As such, HRI provides the ability to perform functional imaging though the quantification of oxyhemoglobin (HbO_2) and deoxyhemoglobin (HHb) concentrations. Key applications of HRI have included burn assessment[12], wound healing[13], retinal exams[14,15], and intra-operative tissue viability assessment[16]. A limited amount of mobile phone-based hyperspectral imagers have been developed in prior

Optics and Biophotonics in Low-Resource Settings IV, edited by David Levitz, Aydogan Ozcan, David Erickson
Proc. of SPIE Vol. 10485, 104850C · © 2018 SPIE · CCC code: 1605-7422/18/$18 · doi: 10.1117/12.2290870

research. While this previous work has proven their feasibility, they have focused primarily on the visible spectrum[17,18], likely due to the limitation of the NIR-blocking filters. As a result, the applications for these hyperspectral imagers has been greatly restricted to fields like food safety[19] and counterfeit bill identification[17], and have not delved into biomedical applications. It is also worth noting that visible HRI oximetry would be limited in penetration depth in most biological tissue (e.g., skin) due to tissue scattering and high Hb absorption, whereas clinical systems tend to use NIR or visible/NIR wavelength combinations to achieve suitable penetration depths[20]. Other work has chosen to bypass the NIR range issue by developing attachments with detectors and filters that allow for HRI imaging at higher resolutions and wider ranges[21]. Additionally, preliminary work toward non-HRI-based oximetry with mobile phone cameras has been investigated with fingertip video measurements for hemoglobin levels[22] and oxygen saturation over a range of 90-100% with an accuracy of ±2%[23].

A variety of phantom-based test method have been developed to help explore these emerging diagnostic imaging tools, since they are particularly useful for device performance comparison and quality control, and can provide referencing to ground truth oxygenation values that may not be possible to obtain *in vivo*. These phantoms are typically made of polymers, hydrogels, or liquid mixtures in idealized forms, with homogeneous or layered structures and basic geometric inclusions. In particular, phantoms for oximetry verification frequently consist of either a liquid mixture of blood and Intralipid or a solid resin or silicone material with defined optical properties, interspersed with channels or a container filled with blood[24,25]. Notably, in one previous study by our group[26], we fabricated a 3D-printed retinal vasculature phantom, containing two layers of simulated vessels filled with blood, for testing of HRI-based oximetry techniques.

The purpose of the current study was to elucidate the effectiveness of mobile phones as quantitative tools for NIR HRI measurements. Specific goals of the study included characterizing the basic performance of mobile phone cameras (i.e., linearity, spectral sensitivity) as measurement tools, and evaluating their capability to measure oxygen saturation across a range of saturation levels, and comparing their accuracy to that of a scientific CCD camera.

2. METHODS

2.1 *Experimental Setup*

In this study, we implemented two NIR-enabled mobile phones and one scientific CCD, with all HRI acquisitions performed with the same tunable light source. This study focuses on evaluation of NIR-enabled mobile phone capability, but does not involve a fully portable device given the large size and power requirements of the tunable light source. The NIR blocking filter had been removed from each phone camera by a third party (Eigen Imaging, Inc., San Diego, California): the first ("Phone #1") was based on an 8-bit CMOS sensor (3264x2448 pixels) with an f/2.4 aperture lens and the second ("Phone #2") was based on a 16-bit CMOS sensor (4032x3024 pixels) with an f/2.2 aperture lens. The phones were held in place with clamps on stable mounts and images were acquired with third-party camera software that allowed the capturing of unprocessed, raw images with fixed exposure and ISO parameters (Phone #1: Camera FV-5, Flavio Gonzalez App-Entwicklung, Stuttgart, Germany; Phone #2: 645 PRO Mk III, Jag.gr, La Colle-sur-Loup, France).

A 16-bit monochrome scientific CCD (1200x1600 pixels, Alta U2000, Apogee Imaging Systems, Roseville, California) with a zoom lens (75 mm focal length, f/3.9, Tamron, Commack, NY) was used to provide a comparison of phone results against a highly quality camera. For the CCD, exposure time was set to 0.5 s while for the phones, ISO and exposure times were set to 100 and 0.25 s, respectively. The tunable external source was a tungsten-halogen lamp (Oriel Instruments, Stratford, Connecticut), delivered through a liquid crystal tunable filter (LCTF, VariSpec SNIR-10-20, CRI, Inc., Waltham, Massachusetts), working in the range of 650 to 1000 nm with a 7-10 nm bandwidth.

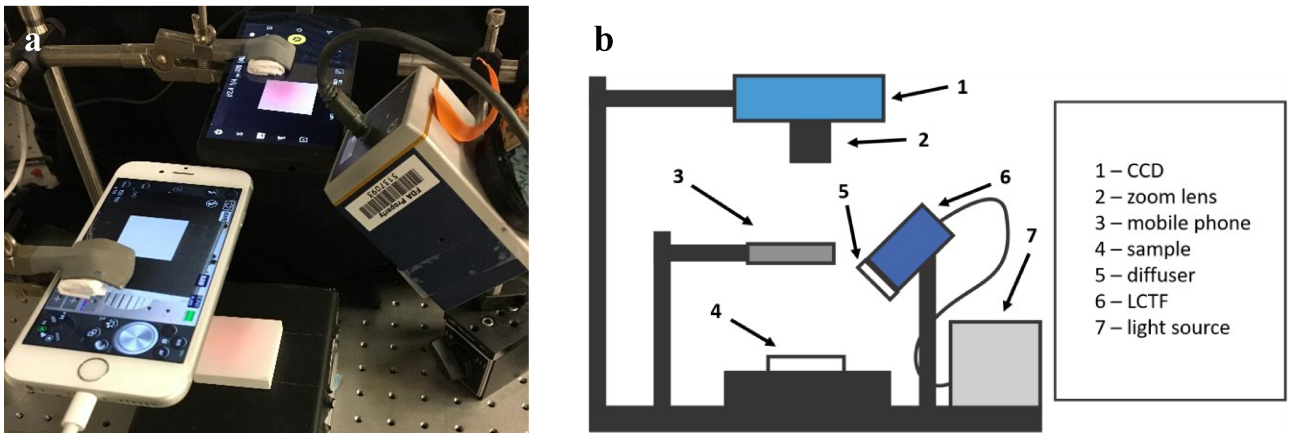

Figure 1. (a) Picture and (b) drawing of the experimental setup.

2.2 *Performance Testing*

Camera spectral sensitivity in the 650-1000 nm range in 10 nm steps was determined through measurements with a diffuse reflectance standard (Spectralon®, Labsphere, Inc., North Sutton, New Hampshire). Irradiance at the standard's surface was measured with a power meter (1918-C Optical Meter, Newport Corp., Irvine, California). Images were taken at each wavelength and then separated into their red, blue, and green constituents. The average signal for a 500x500 pixel region in the center of the standard was calculated and then normalized by the irradiance of the light source (Fig. 2) to determine the spectral sensitivity.

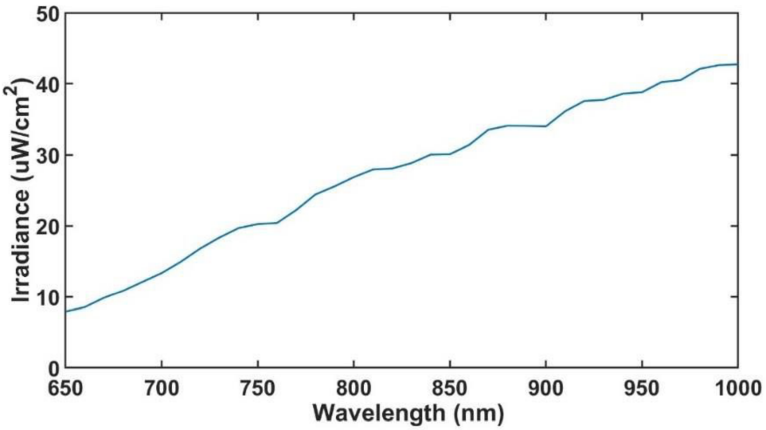

Figure 2. Irradiance spectrum of the LCTF/light source.

To ensure the linear response of the cameras to light intensity, images of the Spectralon® diffuse reflectance standard were taken at five different irradiances and at three different wavelengths (700, 750, and 800 nm). The average signal for a 500 x 500 pixel region in the center of the standard was calculated and a linear regression was performed on this measured intensity vs. the irradiance to determine the linearity of the camera's response.

2.3 *Oximetry Measurements and Data Processing*

A commercially available human HbO_2 solution for calibrating CO-oximeters (Multi-4™ Level 2, Instrumentation Laboratory Co., Bedford, Massachusetts) was used to mimic blood. To fully desaturate the solution, sodium dithionite (Sigma-Aldrich Corporation, St. Louis, Missouri) was added to a concentration of 4 mg/mL. Oxygen saturation (SO_2) was verified by CO-oximeter (Avoximeter 4000, International Technidyne Corp, Edison, New Jersey) and metHb levels were measured to be negligible (~0%). Quartz cuvettes (Starna Cells, Inc., Atascadero, California) were filled with HbO_2 and

HHb solution and sealed with Parafilm (Bemis Company, Inc., Oshkosh, Wisconsin), before being placed on the reflectance standard for imaging with the phone and CCD cameras.

Data were analyzed using custom algorithms written in MATLAB® as follows: (1) Images were median filtered and background subtracted to reduce noise. (2) A 250x250 pixel region of interest (ROI) was selected on the cuvette and a 350x150 pixel ROI on the reflectance standard and the intensity values in those ROIs were averaged for each wavelength. (3) Absorbance for each wavelength was then calculated from the red channel as

$$A(\lambda) = \log(\frac{I_0}{I}) \tag{1}$$

where I_0 is the incident intensity, approximated by the average intensity of the ROI on the reflectance standard, and I is the transmitted intensity, approximated by the average intensity of the ROI on the cuvette.

For a subsequent desaturation experiment, defibrinated bovine blood (Quad Five, Ryegate, Montana) was desaturated with sodium dithionite in four steps, for a total of five saturation levels with metHb <5%. A quartz cuvette was filled with the blood and its absorbance was calculated as above through [Eq. (1)] and the previously described algorithms. The SO_2 of the blood at each saturation level was determined through CO-oximetry and was also solved for by using a non-negative least squares (NNLS) algorithm to determine the fractional contribution of each chromophore (e.g. HbO_2, HHb, water) from the absorbance measured by the phone and CCD over the 650-1000 nm range,

$$\mathrm{A} = [\mathrm{HHb}]\varepsilon_{HHb}L + [\mathrm{HbO_2}]\varepsilon_{HbO_2}L + [\mathrm{H_2O}]\varepsilon_{H_2O}L + \mathrm{Corr}, \quad \min_x\|\mathrm{CX} - \mathrm{A}\| \text{ where } x \geq 0 \tag{2}$$

where ε_x is the known extinction coefficient of the chromophore, [x] is the relative concentration of the chromophore, Corr is a constant correction factor, L is the pathlength, C is the known extinction coefficient matrix, and X is the unknown fractional contribution matrix. SO_2 was then calculated using the HbO_2 and HHb values acquired from the NNLS algorithm through

$$\mathrm{SO_2} = \frac{[\mathrm{HbO_2}]}{[\mathrm{HHb}] + [\mathrm{HbO_2}]} \tag{3}$$

3. RESULTS AND DISCUSSION

3.1 Spectral Sensitivity

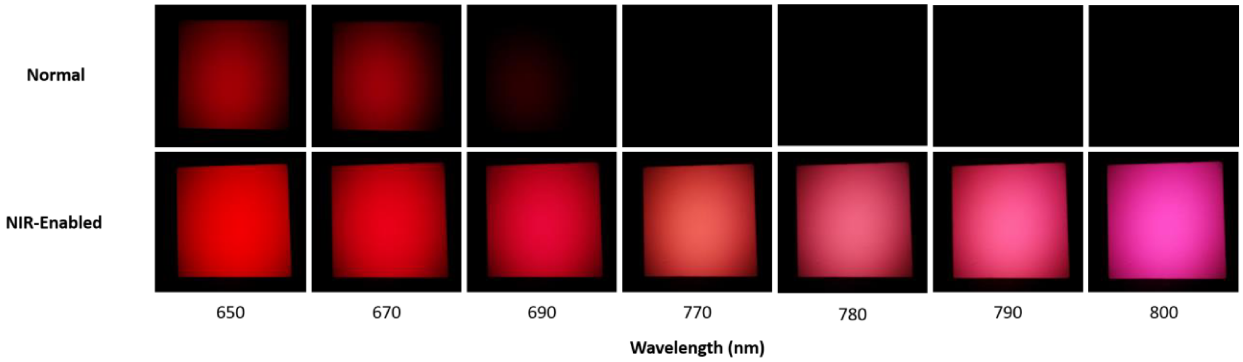

Figure 3. HRI images of a diffuse reflectance standard acquired with Phone #1 ("NIR-Enabled"), compared to its non-NIR-enabled ("Normal") counterpart.

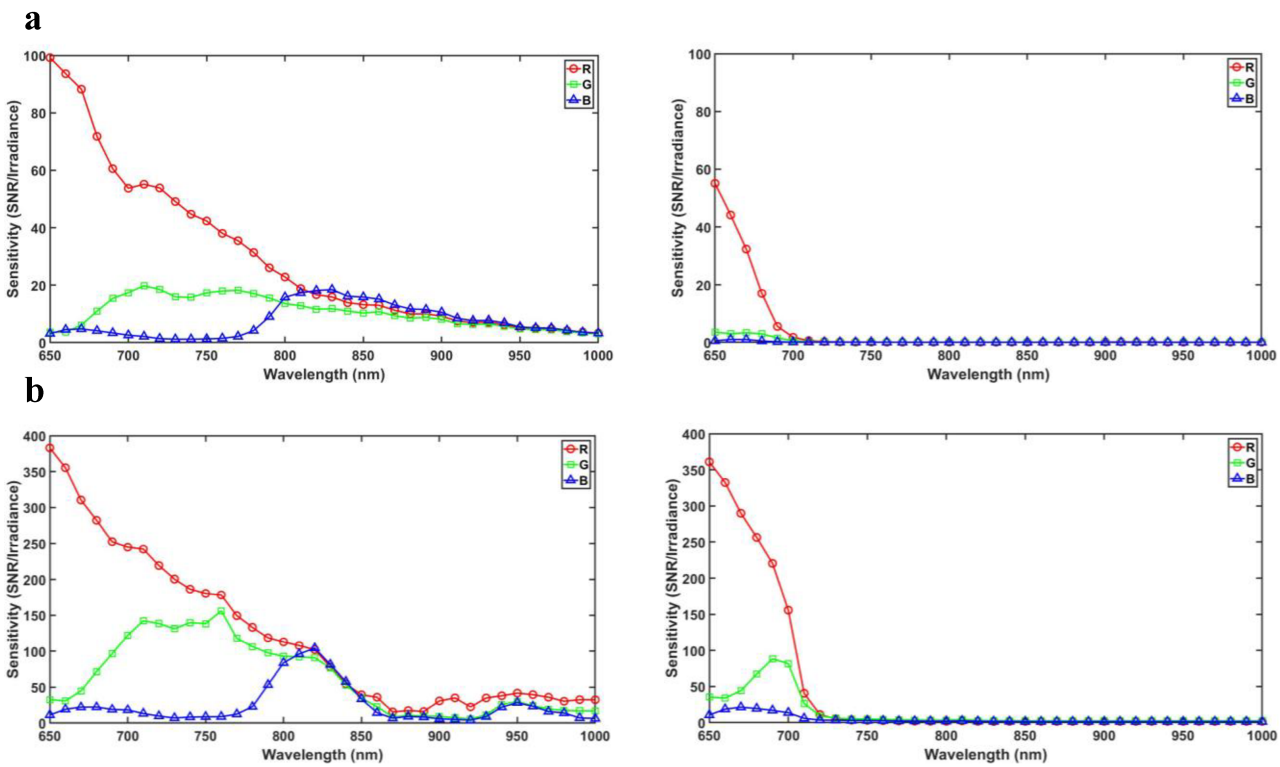

Figure 4. Spectral sensitivity of the red, green and blue pixel channels in (a) Phone #1 and (b) Phone #2 (left), as compared to their non-NIR-enabled counterparts (right). Data normalized to an irradiance of 1 $\mu W/cm^2$.

The spectral sensitivity of the phones with their NIR-blocking filters removed and their standard off-the-shelf counterparts were analyzed (Fig. 4). For both NIR-enabled phones, the red color channel showed the highest sensitivity and decreased monotonically from a high level at 650 nm. Green tended to rise in sensitivity above 650 nm, and blue showed little sensitivity until about 800 nm. At wavelengths above 820 nm, all three color channels begin to have similar sensitivity,

decaying gradually with wavelength. Phone #1 had broad sensitivity spanning the entire tested range (650-1000 nm), while Phone #2 appeared to cut off sharply at around 850 nm, potentially due to a second filter built into the phone. For the off-the-shelf phones (Fig 4, right column), it was clear that a filter was present, with sharp cutoffs at 700 nm and 720 nm for Phone #1 and Phone #2, respectively.

3.2 *Linearity*

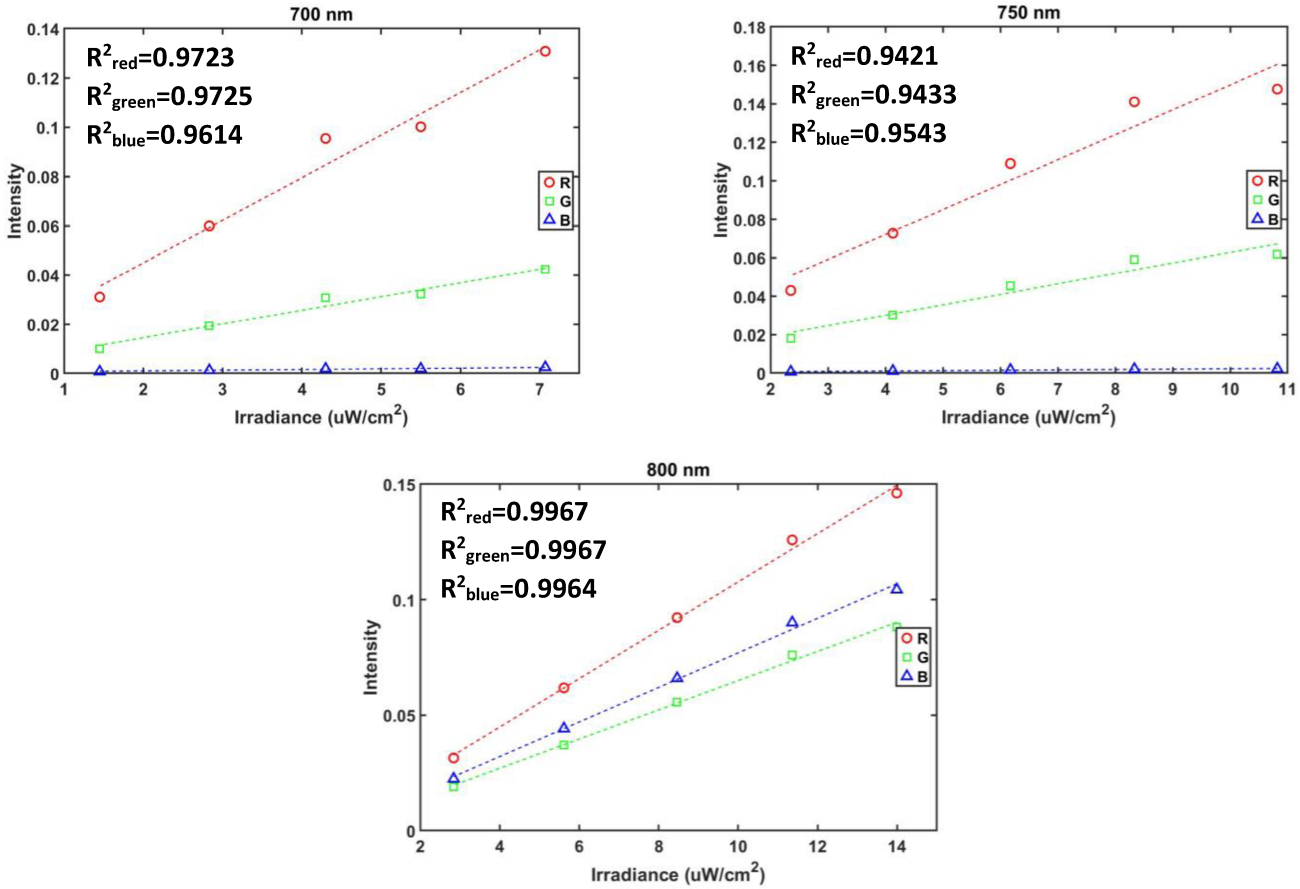

Figure 5. Linearity of the response of the red, green, and blue channels at three wavelengths (700, 750, and 800 nm) for Phone #1 when measuring a diffuse reflectance standard exposed over a range of irradiance levels.

The linearity of each channel's intensity response to changes in light source irradiance for Phone #1 was analyzed through a linear regression and R^2 values were calculated (Fig. 5). The intensity response of Phone #1 overall is highly linear, with R^2 values for each channel > 0.96 at 700 nm, > 0.94 at 750 nm, and > 0.99 at 800 nm.

3.3 *Oximetry*

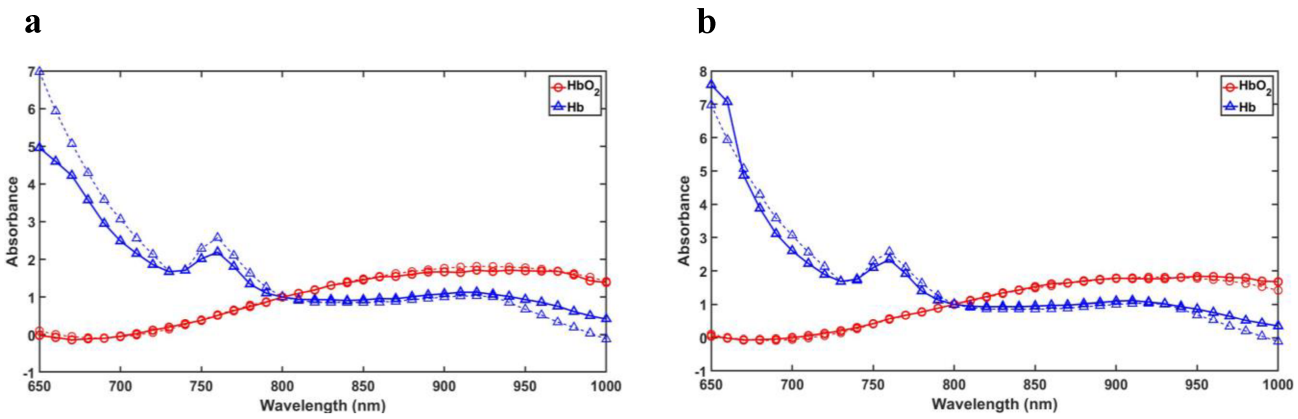

Figure 6. Oxy- and deoxy- hemoglobin normalized absorbance spectra taken in a cuvette by (a) Phone #1 and (b) the scientific CCD, compared to the theoretical spectra, shown with dashed lines.

As a preliminary test, fully oxygenated and fully deoxygenated human Hb solutions were imaged in a cuvette by Phone #1 and the CCD to measure the absorbance spectra (Fig. 6). The measured spectra were compared to theoretical spectra by normalizing at 800 nm to be 1. Both cameras were able to accurately measure HbO_2 absorbance across the spectrum; however, they both measured a slightly higher absorbance in the 900-1000 nm range for HHb, and, in general, a slightly lower absorbance below 800 nm. However, the CCD was better able to match the HHb spectra below 800 nm than Phone #1. Phone #1 was able to determine absorbance spectra with accuracy similar to that of the CCD.

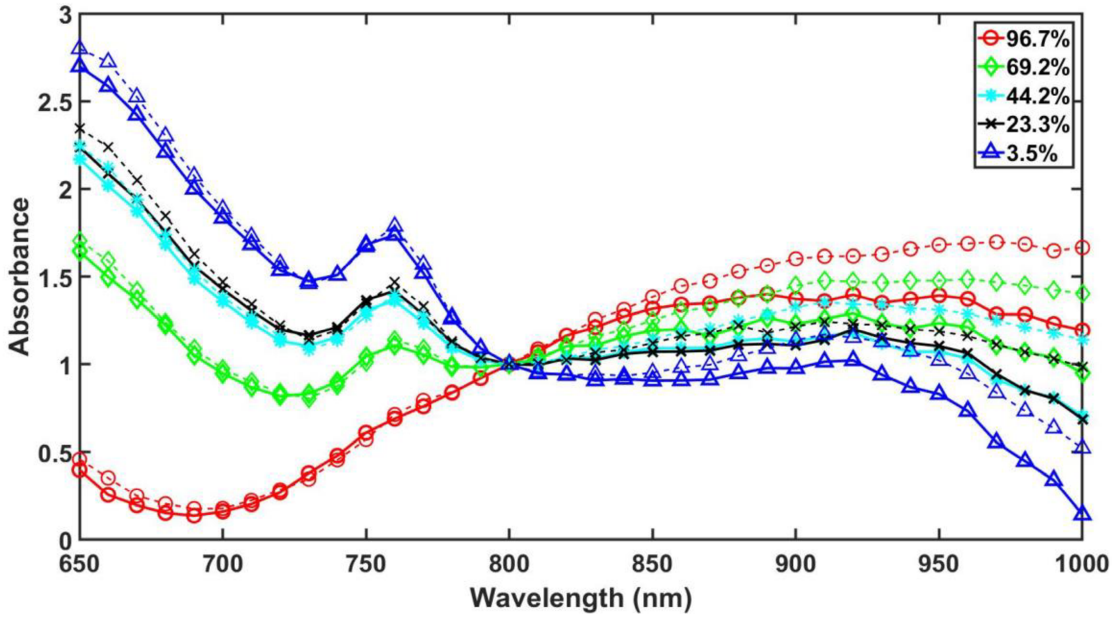

Figure 7. Blood absorbance spectra, normalized at 800 nm, taken in a cuvette for various SO_2 (%) values, as acquired by Phone #1 (solid lines) and the scientific CCD (dashed lines).

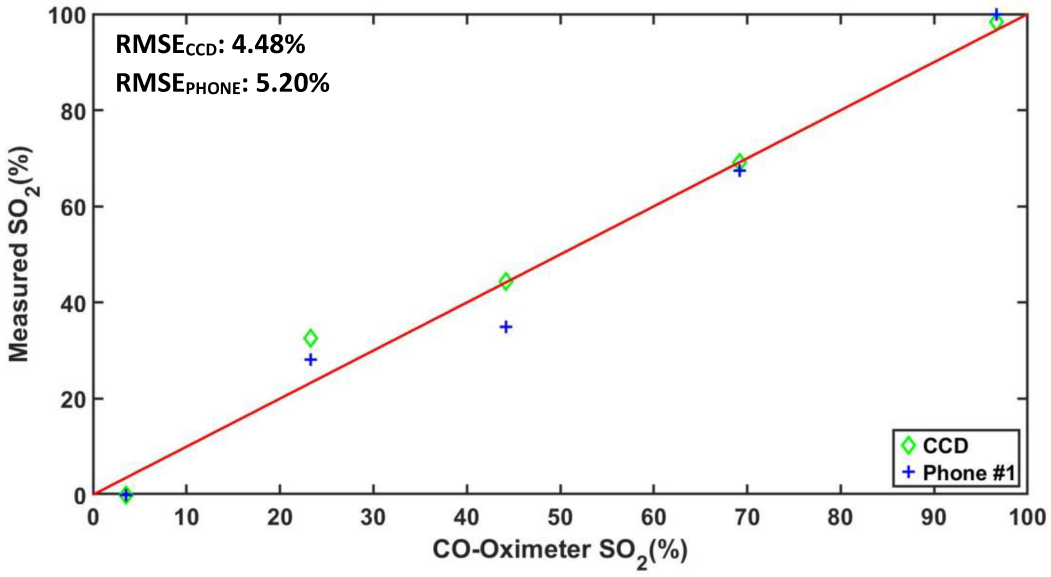

Figure 8. Accuracy of SO_2 values calculated through NNLS [Eq. (2)] from the CCD and Phone #1 spectra in Fig. 7, compared to the CO-oximeter readings.

To further investigate the ability of the NIR-enabled mobile phone to distinguish between saturation levels, blood was desaturated with sodium dithionite to five SO_2 levels and absorbance spectra measured by Phone #1 and the scientific CCD (Fig. 7). Both sets of spectra clearly show the gradual transition from an HbO_2 spectrum to a HHb spectrum, with the deoxyhemoglobin peak around 750 nm becoming more pronounced while the absorbance above 800 nm, where oxyhemoglobin dominates, steadily decreased. The CCD and Phone #1 measured very similar spectra prior to the isosbestic point at 800 nm; however, at longer wavelengths the CCD spectra show higher absorbance values than the spectra measured by Phone #1. This may be due to the lower sensitivity of Phone #1 in this range. Overall, however, Phone #1 was able to perform similarly to the CCD in these spectral measurements.

NNLS [Eq. (2)] was performed on the spectra acquired by both the CCD and Phone #1 to determine the SO_2 (%) measured by each, and compared to values measured by the gold standard CO-oximeter (Fig. 8). The CCD was better able to determine the correct SO_2, closely matching (<5% SO_2 difference) the CO-oximeter reading at all levels, except at 23.3% SO_2 (CO-ox), where it deviated by 32.5%. Meanwhile, Phone #1 diverged from the CO-oximeter readings at two points, at 23.3% (CO-ox) with a value of 28.1% and at 44.2% (CO-ox) with a value of 34.9%. The root-mean-square error of the CCD and Phone #1 results were determined to be 4.5% and 5.2%, respectively. These results indicate an impressive capability of Phone #1 in determination of SO_2 levels compared to the more expensive, higher performance CCD camera.

4. CONCLUSION

We have evaluated the basic feasibility of using NIR-enabled mobile phones as point-of-care diagnostic devices for measuring blood oxygen saturation. Overall, our results provide a proof of principle for mobile phone platforms to be used as quantitative hyperspectral imagers for oximetry, and potentially other applications as well. The primary requirement of a phone camera for clinical use is its ability to acquire RAW images directly from the sensor array of the camera. These are needed to determine the true intensity values read by the camera without any post-processing, such as white balancing. However, not all phones currently have this capability. In addition, variability in camera characteristics, such as spectral sensitivity, between different phone platforms must be considered to ensure consistent performance in oximetry measurements. Ultimately, clinical translation of phone-based systems will require a more compact set of light sources or tunable filter with a broad wavelength range, such as the MEMS FPI-based tunable filters currently in development, and custom processing algorithms for demosaicing and data processing. Future improvements to mobile phone processing power, as well as camera resolution and dynamic range, will also improve their utility as portable instruments for medical care.

ACKNOWLEDGMENTS

The authors gratefully acknowledge funding support from the Food and Drug Administration (FDA) Critical Path Initiative, the National Science Foundation's FDA Scholar-in-Residence program (NSF, CBET-1641077), and the ORISE fellowship program through Oak Ridge Associated Universities. 3D-printing work was performed in the FDA Additive Manufacturing of Medical Products (AMMP) Lab, supported by the Office of the Chief Scientist's Shared Resources program.

Disclaimer: The mention of commercial products, their sources, or their use in connection with material reported herein is not to be construed as either an actual or implied endorsement of such products by the Department of Health and Human Services.

REFERENCES

[1] Chang, J., et al. "Automated Tuberculosis Diagnosis Using Fluorescence Images from a Mobile Microscope." *International Conference on Medical Image Computing and Computer-Assisted Intervention*, Springer, Berlin, Heidelberg, 345-352 (2012).

[2] Suto, S., et al. "Fluorescein fundus angiography with smartphone." *Retina*, **34**, 203-205 (2014).

[3] Maamari, R. N., et al. "A mobile phone-based retinal camera for portable wide field imaging." *Br. J. Ophthalmol.*, **98**, 438-441 (2014).

[4] Scully, C. G., et al. "Physiological parameter monitoring from optical recordings with a mobile phone." *IEEE Transactions on Biomedical Engineering*, **59**, 303-306 (2012).

[5] Lihachev, A., et al. "Autofluorescence imaging of basal cell carcinoma by smartphone RGB camera." *Journal of Biomedical Optics*, **20**, 120502 (2015).

[6] Vashist, S. K., et al. "Commercial Smartphone-Based Devices and Smart Applications for Personalized Healthcare Monitoring and Management." *Diagnostics*, **4**, 104-128 (2014).

[7] Perez, G. M., et al. "Barriers to pilot mobile teleophthalmology in a rural hospital in Southern Malawi." *Pan African Medican Journal*, **19**, (2014).

[8] Ghassemi, P., et al. "Evaluation of mobile phone performance for near-infrared fluorescence imaging." *IEEE Transactions on Biomedical Engineering*, (2016).

[9] Koh, K. R., et al. "Visible and near infrared autofluorescence and hyperspectral imaging spectroscopy for the investigation of colorectal lesions and detection of exogenous fluorophores." *Proc. SPIE 7169, Advanced Biomedical and Clinical Diagnostic Systems VII*, 71691E (2009).

[10] Lindsley, E. H., et al. "The hyperspectral imaging endoscope: a new tool for in vivo cancer detection." *Proc. SPIE 5322, Imaging, Manipulation, and Analysis of Biomolecules, Cells, and Tissues II*, (2004).

[11] Zuzak, K. J., et al. "Characterization of a near-infrared laparoscopic hyperspectral imaging system for minimally invasive surgery." *Anal. Chem.*, **79**(12), 4709-4715 (2007).

[12] Calin, M. A., et al. "Characterization of burns using hyperspectral imaging technique – A preliminary study." *Burns*, **41**, 118-124 (2015).

[13] Nouvong, A., et al. "Evaluation of diabetic foot ulcer healing with hyperspectral imaging of oxyhemoglobin and deoxyhemoglobin." *Diabetes Care*, **32**(11), 2056-2061 (2009).

[14] Nourrit, V., et al. "High-resolution hyperspectral imaging of the retina with a modified fundus camera." *J. Fr. Ophthalmol.*, **33**(10), 686-692 (2010).

[15] Mordant, D. J., et al. "Oxygen saturation measurements of the retinal vasculature in treated asymmetrical primary open-angle glaucoma using hyperspectral imaging." *Eye (Lond.)*, **28**(11), 1190-1200 (2014).

[16] Panasyuk, S. V., et al. "Medical hyperspectral imaging for evaluation of tissue and tumor." *U.S. Patent no. US8320996 B2*.

[17] Rissanen, A., et al. "MEMS FPI-based smartphone hyperspectral imager." *Proc. SPIE 9855, Next-Generation Spectroscopic Technologies IX*, 985507 (2016).

[18] MacKinnon, N., et al. "Melanoma detection using smartphone and multimode hyperspectral imaging." *Proc. SPIE 9711*, 971117 (2016).

[19] Rateni, G., et al. “Smartphone-Based Food Diagnostic Technologies: A Review.” *Sensors*, **17**(6), 1453 (2017).

[20] Zuzak, K. J., et al. “Intraoperative bile duct visualization using near-infrared hyperspectral video imaging.” *The American Journal of Surgery,* **195**(4), 491-497 (2008).

[21] Ishimaru, I., et al. “Built-in hyperspectral camera for smartphone in visible, near-infrared and middle-infrared lights region (first report): Trial products of beans-size Fourier-spectroscopic line-imager and feasibility experimental results of middle infrared spectroscopic imaging.” *Proc. SPIE 9855, Next-Generation Spectroscopic Technologies IX*, 985504 (2016).

[22] Hasan, M. K., et al. “Smartphone-based Human Hemoglobin Level Measurement Analyzing Pixel Intensity of a Fingertip Video on Different Color Spaces.” *Smart Health*, (2017).

[23] Kanva, A. K., et al. “Determination of SpO2 and heart-rate using smart-phone camera.” *2014 International Conference on Control, Instrumentation, Energy and Communication (CIEC)*, IEEE, 237-241 (2014).

[24] Willmann, S., et al. “Small-volume frequency-domain oximetry: phantom experiments and first *in vivo* results.” *Journal of Biomedical Optics*, **8**(4), 618-628 (2003).

[25] Fredriksson, I., et al. “Evaluation of a pointwise microcirculation assessment method using liquid and multilayered tissue simulating phantoms.” *Journal of Biomedical Optics*, **22**(11), 115004 (2017).

[26] Ghassemi, P., et al. “Rapid prototyping of biomimetic vascular phantoms for hyperspectral reflectance imaging.” *Journal of Biomedical Optics*, **20**(12), 121312 (2015).